THE JOURNAL OF PHYSICAL CHEMISTRY A

 VOLUME 111, NUMBER 10, MARCH 15, 2007

ARTICLES

Photochromism of Photoenolizable Ketones in Quinoline and 1,8-Naphthyridine Series Studied by Time-Resolved Absorption Spectroscopy

Stéphane Aloïse,* Julien Réhault, Baptiste Moine, Olivier Poizat, and Guy Buntinx

Laboratoire de Spectrochimie Infrarouge et Raman (UMR 8516 du CNRS), Centre d'études et de recherches Lasers et Applications (FR 2416 du CNRS), Université des Sciences et Technologies de Lille, Bat C5, 59655 Villeneuve d'Ascq Cedex, France

Vladimir Lokshin, Magalie Valès, and André Samat

Groupe de Chimie Organique et Matériaux Moléculaires (UMR 6114), Université de la Méditerranée, Faculté des Sciences de Luminy, Case 901, 13288 Marseille Cedex 09, France

Received: July 12, 2006; In Final Form: January 24, 2007

For the two photochromic molecules, 3-benzoyl-2-benzyl-1-methyl-1H-quinolin-4-one (QC1) and 3-benzoyl-1,2-dibenzyl-*1H*-1,8-naphthyridin-4-one (QC18a) as well as the nonphotochromic 3-benzoyl-1-benzyl-2-methyl-*1H*-1,8-naphthyridin-4-one (QC18b), the full photochemical mechanism, which is based on the photoenolization process, has been elucidated using stationary and time-resolved spectroscopy techniques. After photoexcitation, the $S_1(n,\pi^*)-T_1(n,\pi^*)$ ISC process involving the exocyclic carbonyl chromophore is demonstrated to occur. Subsequently, γ-hydrogen transfer proceeds very rapidly to give rise to the triplet photoenol with a probable 1,4-biradical structure. For all three molecules, the biradical is clearly detected and proved quantitatively to be the direct precursor of the colored form (photochromic compounds) or ground state starting material (nonphotochromic compound). Solvent effects for the three molecules studied may suggest the existence of intramolecular hydrogen bonding in both biradical and colored form species. Structural effects on the γ-hydrogen transfer rate and biradical decay are related to the photochromic performances.

Introduction

The first observation of photochromism in heterocyclic ketones was reported by Ullman et al.[1,2] The phototransformation principle was based on the photoenolization process (Norrish type II reaction) arising in *o*-alkylphenylketones via a [1,5]H sigmatropic shift[3] for which light excitation leads to colored but unstable *o*-xylylenols (ground state photoenol) photoproducts. To obtain photochromic materials with more stable colored forms, Ullman et al. proposed attaching a second carbonyl group to stabilize the enol form via intramolecular hydrogen bonding. This goal was successfully achieved by the replacement of a phenyl nucleus by a heterocyclic analogue possessing an additional carbonyl group. A series of such new compounds were synthesized. Some of them demonstrated photochromic behavior, and the photochemical mechanism was investigated by UV−visible absorption, phosphorescence emission at different temperatures, and deuterium exchange tests.[2] On the basis of this study, the authors suggested that the photochromism results from the occurrence of a thermally activated enolization taking place in an $n\pi^*$ triplet state of the

* To whom correspondence should be addressed. E-mail: stephane.aloise@univ-lille1.fr.

10.1021/jp064397q CCC: $37.00
Published on Web 02/22/2007

SCHEME 1

$$S_0 + h\nu \rightarrow {}^1K \rightarrow {}^3K \rightarrow {}^3E \rightarrow CF$$

CHART 1

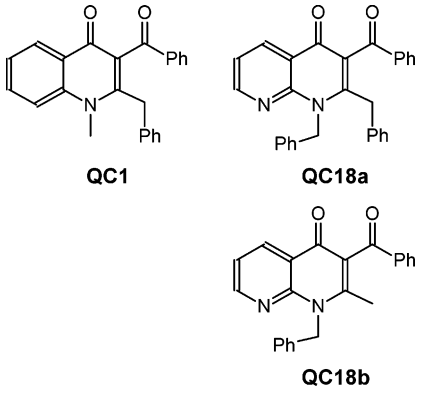

ketonic form (^{3}K). This latter species yields an enol triplet (^{3}E), which relaxes to the colored ground state form (CF) (see Scheme 1).

In fact, this reaction scheme, for which none of the chemical intermediates were directly identified, is in conformity with the well-known general mechanism, which is accepted to describe the photoenolization in simple carbonyl compounds[4,5] such as *o*-benzylbenzophenone[6] or *o*-methylbenzophenone[7] (MBP). Among transient species in photoenolization processes, the triplet photoenol, recognized for a long time to have a 1,4-biradical structure[4,8] (Norrish type II biradical), is of particular importance since its geometry determines the stereoselectivity of the *o*-xylylenol photoproducts.[9]

Recently, renewed interest in the photoenolization processes has emerged because of the possibility of achieving a better stabilization of the photoenol products via hydrogen bonding or electronic control.[10] Within this context and with the final goal of finding new stable photochromic materials,[11] the synthesis of new photoenolizable heterocyclic ketones has been undertaken as a continuation of the initial work of Ullman et al.[1,2] New synthesis routes were found, and approximately 50 compounds were obtained.[12] Preliminary steady state spectroscopic and chemical analyses[12,13] allowed the identification of the compounds, which are photochromic. Among them, two categories of molecules were distinguished depending on whether or not photoenolization is followed by a cyclization step.[13]

The aim of the present paper is to use various time-resolved spectroscopic techniques and standard photochemical methods (solvent and quenching effects) together with steady state absorption experiments under continuous irradiation to obtain better insight into the full photochemical mechanism responsible for the photochromism in these compounds. In particular, it was desired to check the validity of the proposed reaction Scheme 1 by characterizing the different chemical intermediates along the reaction pathway. With regard to this objective, we have chosen to focus our investigation on three molecules (Chart 1) that are representative of the simple photoenolization process (with no postenolization cyclization): 3-Benzoyl-2-benzyl-1-methyl-1H-quinolin-4-one (QC1), already investigated by Ullman et al. by conventional stationary spectroscopic techniques,[1] and two newly synthesized molecules of similar structures, 3-benzoyl-1,2-dibenzyl-1H-1,8-naphthyridin-4-one (QC18a) and 3-benzoyl-1-benzyl-2-methyl-1H-1,8-naphthyridin-4-one (QC18b). As will be seen, the first two are photochromic while QC18b is not. An attempt to understand some structural factors that govern the (non)photochromism of these compounds will be given at the end of this work.

Experimental Section

QC1 was synthesized using a modified procedure,[1] mp 175−176 °C (lit.[1] 177 °C). The synthesis of QC18a was described elsewhere,[12b] and its analogue QC18b was synthesized by the same method. White solid, mp 181 °C (from methanol). ^{1}H NMR ($CDCl_3$): 2.24 (3H, s, CH_3), 5.81 (2H, sl, CH_2), 6.97 (2H, m, H-arom.), 7.12−7.51 (7H, m, H-arom., H-6), 7.81 (2H, m, H-arom.), 8.60 (2H, m, H-5 and H-7). ^{13}C NMR ($CDCl_3$): 18.5 (q), 48.1 (t), 120.5 (d), 120.9 (s), 123.9 (s), 126.0 (d), 127.7 (d), 128.8 (d), 129.1 (d), 129.5 (d), 133.7 (d), 136.1 (d), 136.6 (s), 137.5 (s), 150.7 (s), 151.2 (s), 152.8 (d), 175.7 (s), 196.6 (s). Anal. calcd for $C_{23}H_{18}N_2O_2$: C, 77.95; H, 5.12; N, 7.90. Found: C, 78.10; H, 5.10; N, 7.83.

For the spectroscopic experiments, used were the following spectroscopic grade Sigma-Aldrich products: acetonitrile (CH_3-CN), methanol (CH_3OH), dimethylsulfoxide (DMSO), and trifluoroethanol (TFE). All solvents were used without further purification.

The pump−probe subpicosecond absorption experiments were carried out using an amplified Ti:sapphire laser (BMI Industry) delivering 0.8 mJ and 80 fs pulses at 800 nm with a repetition rate of 1 kHz. The pump pulses were obtained by frequency tripling the fundamental giving 30 μJ pulses at 266 nm. The probe beam was generated by focusing 1 μJ of the fundamental on a 1 mm CaF_2 plate giving a white light continuum with a spectrum covering the UV−vis and near IR range. The probe beam was split into signal and reference beams before crossing the sample, and the resulting beams were recorded on two different channels of a multichannel spectrograph. Transient absorbance was obtained by comparing signal and reference spectra for different time delays. The time delay between the pump and the probe could be varied by up to 1.5 ns (using a micrometric optical delay line), and the temporal resolution of the apparatus was better than 300 fs. Pump and probe beams, with relative linear polarizations at the magic angle, were focused in a 2 mm flowing sample cell with CaF_2 windows. The typical sample concentration used was 5×10^{-4} M.

A conventional laser flash photolysis apparatus was used to record nanosecond time-resolved absorbance data. Pump pulses (355 nm) of 7 ns and 1 mJ delivered by a nanosecond diode-pumped Q-switched laser (Thales) were focused onto a 10 mm optical path sample cell. The probe light was provided by a xenon lamp and analyzed with a photomultiplier via a spectrometer coupled to a digitalized oscilloscope (TDS540, Tektronics). This system allows a 50 ns time resolution. All solutions were prepared in such a way that the stationary optical density at 355 nm is about unity. Furthermore, all solutions were degassed by bubbling N_2. The quenchers *cis*-1,3-pentadiene and paraquat (Sigma-Aldrich) were used as received, and the latter was dissolved in wet acetonitrile (9:1). Quenching by O_2 was achieved by simply bubbling the gas through the deaerated solutions.

Steady state photolysis experiments were performed in a thermostated at 20 °C (±0.2 °C) copper block inside the sample chamber of a Cary 50 spectrometer. The optical path length of the cell was 10 mm. An Oriel 150W high-pressure Xe lamp was used for irradiation, and excitation wavelengths were selected by a monochromator tuned to the maximum absorbance of the uncolored form.

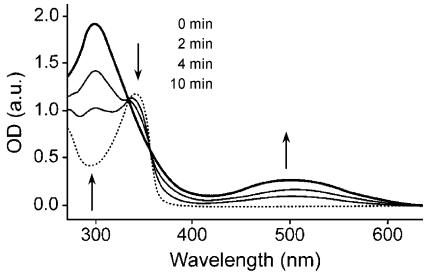

Figure 1. Absorption spectra of QC18a in acetonitrile under continuous UV irradiation acquired at different times as indicated on the graph.

TABLE 1: Spectrokinetic Parameters Obtained from Stationary Absorption Experiments for QC1, QC18a, and QC18b in Acetonitrile

	λ_{max}(nm)			
	uncolored form	colored form	k_Δ (s^{-1})	E_a (kJ mol^{-1})
QC1	338	490	2.6×10^{-3}	55.8 ± 0.9
QC18a	339	500	6.3×10^{-3}	55.3 ± 0.5
QC18b	338			

Results

Steady State Photolysis Experiments. UV−vis absorption spectra through continuous illumination acquired at regular temporal steps are shown for QC18a in acetonitrile in Figure 1. The initial spectrum, recorded in the absence of illumination, is due to the uncolored species (typical band at 339 nm). Subsequently, a gradual evolution is seen with irradiation time, with two clear isosbestic points at 330 and 355 nm, which gives evidence of the photochromic transformation. The final spectrum recorded after 10 min of irradiation shows a visible absorption band that corresponds to the colored form CF. Similar spectra and temporal behaviors were obtained for the QC1 molecule (not shown). The absorption maximum of CF in the visible region stands at 486 and 500 nm for QC1 and QC18a, respectively (Table 1). It provides a spectral reference for identifying the colored form in time-resolved data. In contrast to QC1 and QC18a, QC18b does not present any spectral evolution upon continuous photoexcitation, revealing the absence of photochromic behavior in this molecule. As thermal reversibility is an essential parameter of the photochromism effect, we have examined the ability of CF to return to the uncolored molecule when the irradiation is stopped. Indeed, by measuring the kinetic evolution at the characteristic CF absorbance, we observe that both QC1 and QC18a undergo a back reaction in the dark with thermal fading rates, k_Δ, of a few min^{-1}. By varying the temperature of the sample, the activation energy E_a of this fading process could also be determined. All of these spectrokinetic properties are summarized in Table 1.

Subpicosecond Time-Resolved Absorption Measurements. For QC18a in acetonitrile, transient absorption spectra recorded in the 320−690 nm spectral range within time windows of 2−10 and 20−500 ps following 267 nm excitation are shown in Figure 2a,b, respectively. The strong negative signal near 340 nm is due to bleaching as it corresponds to the λ_{max} of the uncolored form (see Table 1). This signal is nearly constant at all times, indicating that no significant repopulation occurs on this time scale. Apart from this bleaching signal, the shortest time spectrum (2 ps) is characterized by a UV-blue absorption peaking at 365 nm that will be ascribed in the following to a state named S. A rapid overview of the 2−10 ps spectral evolution shows the decrease of the 365 nm band while no increasing signal can be detected. Subsequently, in the 20−500 ps time domain, another type of spectral evolution occurs, which is characterized by concomitant absorption growths at $\lambda_{max} = 405$ and 655 nm and absorption decays in the 350−380 and 420−450 nm regions. The resulting spectrum is assigned to a new intermediate state named T_B. However, it is clear that the band S is not the direct precursor of the band T_B. Indeed, as it can be seen from Figure 3a), the absorption kinetic behavior at 365 nm is well-fitted with a biexponential function with decay times of 12 (band S decay; 68%) and 180 ps (decays of an intermediate species; 32%). On the contrary, the kinetics at 655 nm (band T_B growths) can be fitted by a monoexponential function with the same 180 ps characteristic time. The simpler way to describe our results is to assume a two-step process, S → T_A and T_A → T_B, even if it appears difficult to isolate clearly the new T_A intermediate. The second step of this mechanism is supported by the presence of one real isosbestic point at 417 nm that reveals the participation of two species kinetically linked (see the inset in Figure 2b). During the kinetic evolution, the shoulder peaking near $\lambda_{max} = 413$ nm (see the 20 ps trace) evolves until the new maximum, $\lambda_{max} = 405$ nm attributed to the band T_B, is reached (see the 500 ps trace). The 413 nm

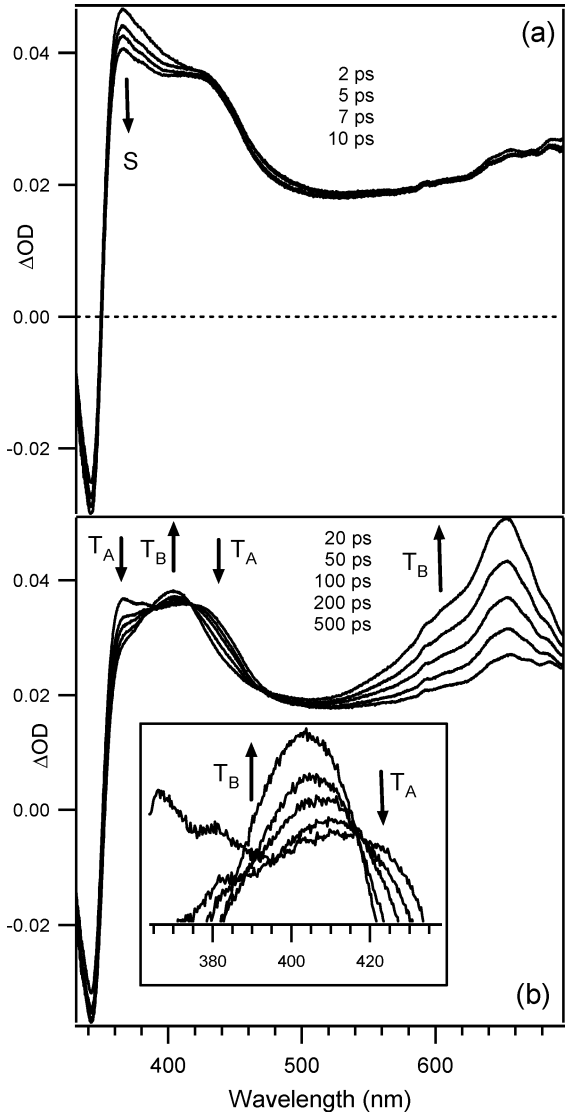

Figure 2. Subpicosecond time-resolved absorption spectra (267 nm excitation) of QC18a in acetonitrile in the 2−10 (a) and 20−500 ps (b) time domains. The time evolution is shown by arrows, and the band assignments to S, T_A, and T_B species are indicated. The inset is a zoom of the 365−465 nm region.

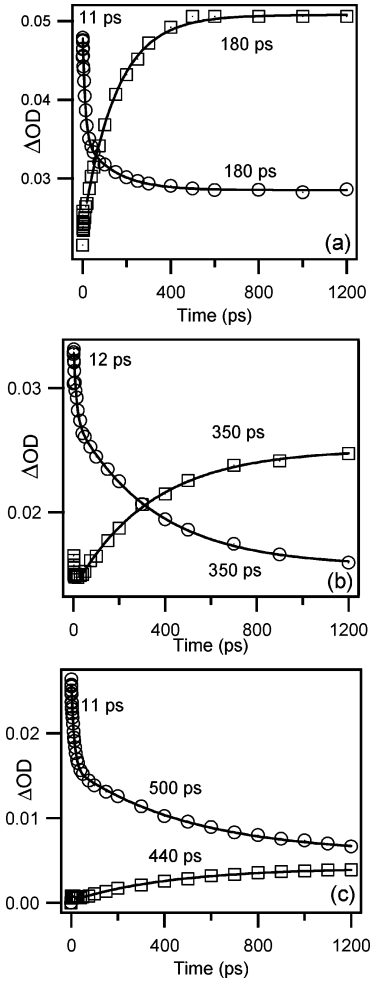

Figure 3. Kinetics obtained in acetonitrile during the 0−1200 ps time window at: (a) 365 (○) and 655 nm (□) for QC18a, (b) 365 (○) and 660 nm (□) for QC18b, and (c) 350 (○) and 640 nm (□) for QC1; in this latter case, the kinetics at 640 nm is obtained after subtraction of the kinetics of the background monitored at 560 nm. Solid lines are the results of exponential fitting.

TABLE 2: Spectral and Kinetic Data Defining Transient Species S, T_A, and T_B Detected during Subpicosecond Time-Resolved Absorption Experiments for QC1, QC18a, and QC18b (in Acetonitrile)[a]

	λ_{max} (nm)			τ_S (ps)	τ_1 (ps)
	S	T_A	T_B	$S \rightarrow T_A$	$T_A \rightarrow T_B$
QC18a	365	413	405 655	11 ± 2	180 ± 20
QC18b	365	425	404 660	12 ± 2	350 ± 40
QC1	350	-	395 640	12 ± 1	440 ± 30

[a] τ_S and τ_1 are the lifetimes of S and T_A, respectively.

band is therefore ascribed to T_A. In the following, lifetimes (decay rate constants) of S and T_A species will be denoted by τ_S (k_s) and τ_1 (k_1), respectively. For the three species S, T_A, and T_B, the λ_{max} and kinetic parameters are reported in Table 2.

For QC18b (spectra not shown), quite an identical spectral and kinetic behavior is found (see Table 2). Indeed, as shown in Figure 3b, the 365 nm kinetics displays a fast decay (12 ps; 33%) attributed to the S intermediate (λ_{max} = 365 nm) and a longer one (350 ps; 67%) attributed to the T_A intermediate. This latter time holds also for the growth of T_B (λ_{max} = 404 and 660 nm) monitored at 660 nm. The maximum of absorption of the

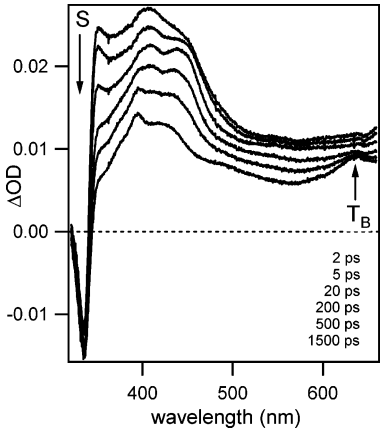

Figure 4. Subpicosecond time-resolved absorption spectra (267 nm excitation) of QC1 in acetonitrile in the 2−1500 ps time domain.

T_A species, determined as above, gives a maximum of absorption at λ_{max} = 425 nm. Note that the T_A lifetime (Table 2) is a factor of about two larger as compared to the value found in the case of QC18a.

Finally, for QC1, the spectral evolution (Figure 4) is somewhat less clear since no rising component is observed due to the presence of an additional decreasing broad background signal. However, common points with QC18a and QC18b molecules can be found. The absorption kinetics at 350 nm (λ_{max}) shown in Figure 3c can be still fitted with a biexponential function with decay times of 12 (50%) and 500 ps (50%). As previously, the shorter time can be assigned to the decay of the S species by analogy with QC18a and QC18b. Furthermore, the final spectrum (1500 ps) shows a weak absorption band near 640 nm and two maxima at 390 and 425 nm that can be considered to be analogous to the T_B bands in the above two compounds although their relative intensities appear quite different. A growth time of 440 ps can be estimated for the 640 nm band by subtracting the kinetics of the background monitored at 560 nm from the kinetics at 640 nm as shown in Figure 3c. This time correlates approximately to the longest decay time (500 ps) found at 350 nm and is therefore attributed to the growth of the T_B intermediate. In the case of QC1, the absence of isosbestic point makes the spectral identification of T_A difficult. No attempt to explain the additional decreasing background will be given in the following.

Finally, to better rationalize the initial photochemical events in the three studied molecules and to facilitate appropriate comparisons, time-resolved absorption measurements were also made on the photoenolizable MBP as well as the benzophenone (BP) molecule to obtain kinetic data under the same experimental conditions (see Discussion).

Nanosecond Laser-Flash Photolysis Experiments. Laser flash photolysis experiments were performed for 355 nm laser excitation in various deaerated solvents. The spectra recorded for QC1 in acetonitrile in the 340−670 nm spectral domain are displayed in Figure 5. Note the bad signal-to-noise ratio below 340 nm that prevents a good acquisition of the bleaching signal (expected at 338 nm). At short times (70 ns), the spectrum corresponds to that observed above for T_B (1500 ps trace in Figure 4) with absorption bands at 390 and 640 nm. This spectrum decreases exponentially with a characteristic time of 255 ns (value measured at 640 nm) until a final spectrum is observed with a peak at 355 nm and a broad band around 490 nm. This last spectrum is characteristic of the colored form (CF) identified in the steady state measurements (see Table 1).

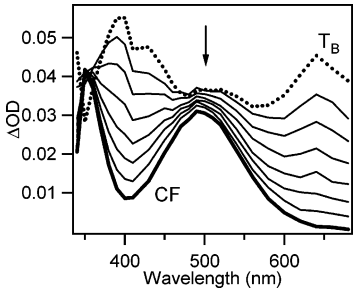

Figure 5. Laser flash photolysis spectra (355 nm excitation) obtained for QC1 in acetonitrile between 340 and 680 nm. The arrows indicate the evolution of the spectra. The delay times are 0.06 (dashed line), 0.14, 0.2, 0.28, 0.38, 0.5, 0.7, and 1.6 μs (bold).

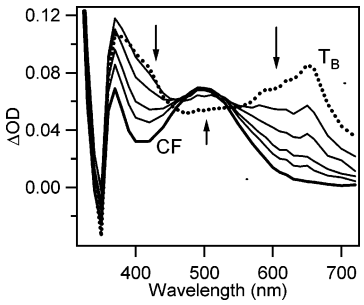

Figure 6. Laser flash photolysis spectra (355 nm excitation) obtained for QC18a in acetonitrile between 320 and 720 nm. The arrows indicate the evolution of the spectra. The delay times are 0.06 (dashed line), 0.09, 0.12, 0.16, 0.20, and 1.6 μs (bold).

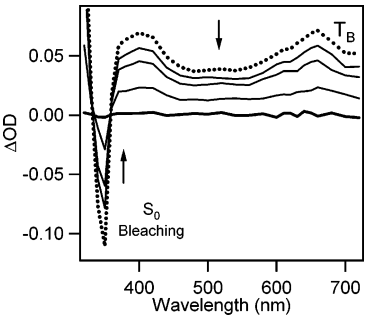

Figure 7. Laser flash photolysis spectra (355 nm excitation) obtained for QC18b in acetonitrile between 320 and 720 nm. The arrows indicate the evolution of the spectra. The delay times are 0.06 (dashed line), 0.14, 0.2, 0.4, and 1.6 μs (bold).

For QC18a, as shown in Figure 6, besides the clear bleaching signal around 340 nm, the spectrum of T_B is clearly identified by comparison with the picosecond data (see the 500 ps trace in Figure 2b) and seems to lead to the CF species (see Figure 1 and Table 1) within 45 ns. However, as in the case of QC1, the kinetic sequence $T_B \rightarrow$ CF is not supported by the presence of unambiguous isosbestic points (only a slight rising component is noticed around 500 nm). This kinetic sequence will be confirmed below by quenching experiments.

Finally, for QC18b (Figure 7), the T_B spectrum can still be observed at short times, but unlike the two other molecules, it disappears completely with a characteristic time of 285 ns without yielding any new absorption signal. The 340 nm bleaching signal disappears simultaneously with the same time constant, and clear isosbestic points are observed near 330 and 360 nm. These observations indicate clearly that T_B relaxes to the ground state instead of producing the colored form, in agreement with the fact that no photochromism was observed for QC18b from steady state measurements. For the three

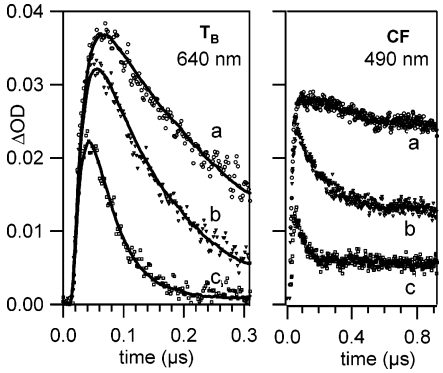

Figure 8. Kinetics obtained from laser flash photolysis at 640 (left) and 490 nm (right) for QC1 in wet acetonitrile for increasing concentrations of *cis*-1,3-pentadiene: (a) no quencher, (b) 0.004 M, and (c) 0.023 M. Bold lines are fitting curves.

TABLE 3: Lifetimes (τ_2) and Quenching Rate Constants (*cis*-1,3-Pentadiene and Paraquat) of Transient Species T_B Obtained from the Laser Flash Photolysis Experiment

	τ_2 (ns)[a]	k_2^Q (10^9 M^{-1} s^{-1})[a]	$k_2^{PQ^{2+}}$ (10^9 M^{-1} s^{-1})[b]
QC1	255 ± 5	0.86 ± 0.05	10.1 ± 0.3
QC18a	45 ± 1	1.74 ± 0.02	
QC18b	285 ± 3	1.72 ± 0.04	7.5 ± 0.6

[a] In acetonitrile. [b] In wet acetonitrile.

molecules, the lifetime (decay rate) of the T_B species, denoted τ_2 (k_2), is reported in Table 3.

Quenching Results. To gain more information about the T_B species, we studied the effect of different types of quenchers. First, we observed for the three molecules a clear shortening of the T_B lifetime in the presence of oxygen in the solution, indicating either a triplet[14] or biradical nature for this species (biradicals are known to be very sensitive to paramagnetic substances[5,15]). Next, as shown for example for QC1 in Figure 8, adding 1,3-pentadiene also shortens the T_B decay time (640 nm kinetics) and reduces simultaneously the final CF yield (as measured by the intensity of the long time "plateau" absorption at 490 nm). Note that the 640 nm kinetics is well fit by a monoexponential function convoluted with the apparatus response function.[16] Therefore, on the one hand, the triplet nature of T_B is thus confirmed while on the other hand T_B seems to be a precursor of the CF species. We can prove quantitatively that these two species are directly related. As seen in Figure 9a for the three molecules, the observed decay rate, k_{exp}, at 640 nm depends linearly on the quencher concentration according to the Stern−Volmer equation:

$$k_{exp} = k_2 + k_2^Q[Q] \quad (1)$$

The corresponding quenching rate k_2^Q values are given in Table 3. On the other hand, in the above assumption that T_B is the direct precursor of CF (QC1 and QC18a), the intensity of the long time absorbance plateau at 490 nm (A_∞^Q) is also expected to vary linearly with the inverse of the quencher concentration according to:

$$\frac{A_\infty^0}{A_\infty^0 - A_\infty^Q} = 1 + \frac{k_2}{k_2^Q} \cdot \frac{1}{[Q]} \quad (2)$$

where A_∞^0 is the final absorption at 490 nm in the absence of 1,3-pentadiene. Linear fits are indeed observed for both QC1 and QC18a (Figure 9b) and lead to values of the slope of 0.0043

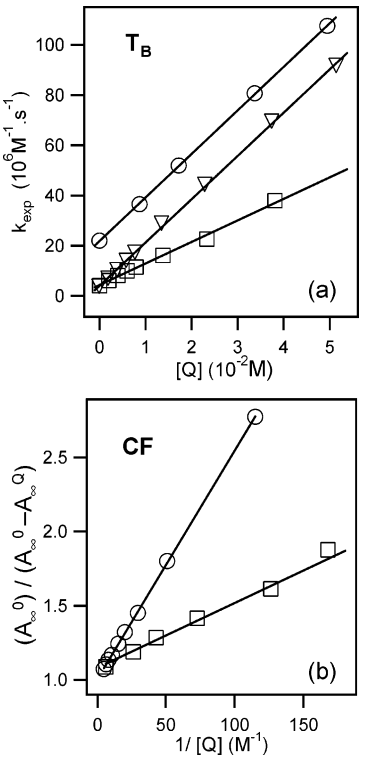

Figure 9. Sterm−Volmer plots concerning QC1 (□), QC18a (○), and QC18b (▽) in acetonitrile solvent. (a) Experimental decay rate, k_{exp}, of T_B species (eq 1) obtained from kinetics at 640 nm wavelength detection (Figure 8, left) function of 1,3-pentadiene concentration [Q]. (b) Calculated ratio (eq 2) obtained from long time plateau absorbance of CF (QC1 and QC18a only) at 490 nm wavelength detection (Figure 8, right) function of the inverse of quencher concentration.

and 0.015, respectively, in excellent accordance with the k_2/k_2^Q ratios of 0.0045 and 0.013, respectively, calculated from the values found from the 640 nm fits (Table 3). This result definitively confirms the sequence:

$$T_B(\sim 640\ \text{nm}) \rightarrow CF(\sim 490\ \text{nm}) \qquad (3)$$

As photoenolization processes are known to involve 1,4-biradicals,[5,8] the effect of adding paraquat PQ^{2+} (methylviologen), which is one of the best quenchers of such biradicals,[17] has also been checked following the method[17] given by Das et al. Effective quenching was observed for all three compounds, but quenching constants of the T_B intermediate (see Table 3) were obtained quantitatively only for QC1 and QC18b because of the too short T_B lifetime of QC18a. These last results indicate that T_B is a biradical species.

Solvent effects. To identify enol type products among the transient species involved in the photoenolization process, solvent influence has been tested. Indeed, as first demonstrated by Haag et al. in the case of simple photoenolizable compounds,[18] lifetimes of photoenols in the singlet or triplet manifold are substantially enhanced in solvents having strong hydrogen bond acceptor (HBA) basicity (related to the β parameter[19] that measures the solvent's ability to accept a proton in a solute-to-solvent hydrogen bond). Such an effect, explained by a better solvation of the enol function,[18] is usually not accompanied by any spectral modification. In the present case, various unexpected results were obtained. First, for the three molecules, the T_B triplet species lifetime measured at 640 nm does not display any enhancement with the HBA basicity of the solvent as shown in Table 4. In fact, almost the opposite situation occurs since a maximum lifetime is obtained for CH_3CN, which has a moderate HBA basicity value as compared to DMSO. Then, in the case of the CF species, a drastic hypsochromic shift is observed as a function of the increasing HBA basicity of the solvent. In Figure 10, the CF spectrum of QC18a acquired at 1600 ns peaks at 505, 500, 480, and 440 nm in TFE, CH_3CN, CH_3OH, and DMSO, respectively. A similar effect is found for QC1, and all values are reported in Table 4. Therefore, it is clear that the general approach given by Haag et al. cannot be applied directly for the molecules studied here and the apparent discrepancies will be discuss in the following section.

TABLE 4: Spectrokinetic Parameters Related to the CF (λ_{max}) and T_B Species (Lifetime) for Various Solvents[a]

		QC**1**		QC**18a**		QC**18b**
	β[b]	CF λ_{max} (nm)[c]	T_B τ_2 (ns)[d]	CF λ_{max} (nm)[c]	T_B τ_2 (ns)[e]	T_B τ_2 (ns)[e]
TFE	0.00	510	190	505	15	15
CH_3CN	0.31	490	255	500	45	285
CH_3OH	0.62	470	135	480	15	70
DMSO	0.76	450	160	440	20	40

[a] HBA basicity parameters (β) are indicated. [b] From ref 18. [c] ±5 nm. [d] ±5 ns. [e] ±3 ns.

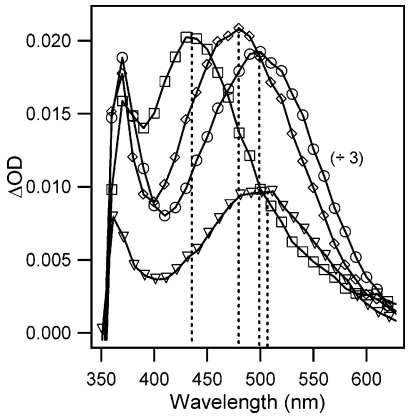

Figure 10. Laser flash photolysis spectra of the QC18a molecule in DMSO (□), CH_3CN (○), CH_3OH (◊), and TFE (▽) for time delays Δt = 1600 ns (CF species). Scaling factors concern the acetonitrile case.

SCHEME 2

QC1 and QC18a: $S_0 + h\nu \rightarrow S \rightarrow T_A \rightarrow T_B \rightarrow CF$

QC18b: $S_0 + h\nu \rightarrow S \rightarrow T_A \rightarrow T_B \rightarrow S_0$

To obtain a synthetic view of the kinetic mechanism, the reaction Scheme 2 summarizes the results obtained for the three molecules from the femtosecond and nanosecond measurements including the quenching experiment results.

Discussion

Our results reveal extensive analogies between the reaction Scheme 2 proposed for the studied compounds and the reaction Scheme 1 suggested by Ullman et al. since the same number of reaction intermediates are involved in both cases. In light of the agreement between both schemes, we propose in the following to identify all of the species involved in the photochemical process. After some comments about the CF compound and the global photochromic process, first the transient species T_B will be discussed and then the species S and T_A. After discussing the full photochemical mechanism, additional comments concerning the structural factors that influence the photochromism will end this section.

SCHEME 3

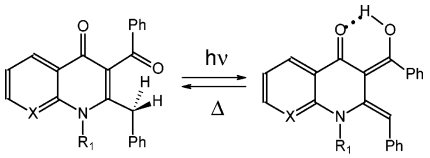

Colored Form Species Stabilized by Intramolecular Hydrogen Bonding. First, as suggested by Ullman et al.,[1,2] the final product for the photochromic heterocyclic ketones has to be the same type of ground state *ortho*-xylylenol, thermally unstable in most common ketones but stabilized by intramolecular hydrogen bonding for the colored form CF in the case of QC1 and also for QC18a compounds. In fact, the global photochromic mechanism (Scheme 3) postulated in the past has only recently been confirmed by structural analysis using the time-resolved NMR technique.[20] From the present results, the stabilization of the colored forms, i.e., the ground state photoenols, is first confirmed by the comparison of its lifetimes, in the order of few minutes (Table 1), with the 2.9 ms value reported for the most stable photoenol of MBP[7] (trans isomer).

Furthermore, the unexpected and drastic hypsochromic effect observed on increasing the HBA character of the solvent (Figure 10) is probably related to the presence of the enol function stabilized by an intramolecular hydrogen bond. Indeed, progressively stronger hydrogen bond acceptor solvents compete more and more efficiently with the initial intramolecular hydrogen bond, which decreases the planarity of the CF molecule and consequently the extension of the electronic π-conjugation system. This effect can therefore explain the observed blue shift of CF spectra upon increasing the β-parameter. Such a competition between intra- and intermolecular hydrogen bonds inducing a blue shift has been reported for the 2-hydroxybenzophenone,[21] which supports the hypothesis outlined above. If this interpretation is correct, the hypsochromic shift could be taken as a particularly elegant signature of the presence of an intramolecular hydrogen-bonded enol group in the colored form species.

Identification of the T_B Species. In this section, we will discuss the nature of the direct precursor of the CF species. It has been clearly shown using a Sterm−Volmer approach (see eqs 1−3) that this precursor is the T_B species. The latter has been identified as the 1,4-biradical species (oxygen and paraquat quenching) frequently invoked during the photoenolization process displaying an excited triplet state behavior[23,24] (oxygen and 1,3-pentadiene quenching).

If the T_B species is recognized as being the 1,4-biradical intermediate, it implies that the $T_A \rightarrow T_B$ kinetic step corresponds to the [1,5]H sigmatropic shift. On the other hand, the rate of γ-hydrogen transfer is known to depend on the nature of the intramolecular hydrogen donor group.[25] In our case, the appearance rate of the T_B intermediate (i.e., $k_1 \approx 1/\tau_1$; see Table 2) is reduced by a factor of about two on going from QC18a to QC18b in accordance with the fact that the γ C−H bond is more weakened by the adjacent phenyl than by the adjacent hydrogen substituent. This structural effect is therefore in accordance with the above assignment.

The lack of enhancement of the T_B lifetime in strong HBA solvents (Table 4), which appears to be in contradiction with the prediction of Haag et al., can be explained by the fact that the solvation of the enol group by intermolecular hydrogen bonding cannot take place. Indeed, as in the case of CF species, the enol group may already be stabilized by intramolecular hydrogen bonding.

In summary, for the T_B intermediate, reliable information has been obtained about the triplet multiplicity, the biradical nature, and the occurrence of an enol group engaged in intramolecular hydrogen bonding. Accordingly, we can denote this species as ^{3}BR-E, notation that summarizes more precisely the three above characteristics of T_B in comparison with the ^{3}E notation found in the Ullman et al. reaction scheme (Scheme 1).

Identification of the S and T_A Species. At this point, it is desirable to characterize more precisely the two prior precursors of ^{3}BR-E noted S and T_A. In this regard, it is interesting to compare our time-resolved spectroscopic data on the photophysics of QC1, QC18a, and QC18b with similar data reported for typical molecules undergoing such photoenolization processes (e.g., MBP[7]) that have been studied by ultrafast absorption spectroscopy. Data concerning the photophysics of the neighboring benzophenone molecule (BP)[26] that does not undergo photoenolization are also worthy of comparison. After photoexcitation, the lowest excited singlet state $S_1(n,\pi^*)$ of BP as well as MBP relaxes through an ISC process to the first triplet state $T_1(n,\pi^*)$ with characteristic times of between 10 and 13 ps for BP in acetonitrile[26] and 5 ps for MBP in ethanol solvent.[7] Under our experimental conditions and in acetonitrile solvent, we found values of 11 ps for BP and 12 ps for MBP. By comparing these two characteristic lifetimes with the ones in Table 2, one can deduce that the (n,π^*) nature of the BP S_1 state is maintained in all molecules. Thus, the precursor S can be assigned to the first excited state $S_1(n,\pi^*)$ (^{1}K in Scheme 1) while the T_A state can be ascribed to the $T_1(n,\pi^*)$ state (^{3}K in Scheme 1). As in the case of MBP, because the hydrogen transfer has not yet occurred, a keto structure is assumed for $T_1(n,\pi^*)$.

Full Photochemical Mechanism. Having identified all transient species, the full photochemical mechanism of the photoenolizable heterocyclic ketones, displayed in Figure 11, can now be discussed. After the photooexcitation, the $S_1(n,\pi^*)$ state relaxes through an ISC process to the first excited triplet state $T_1(n,\pi^*)$. The photophysics engaged at this stage, localized on the exocyclic carbonyl, mimics the BP behavior. In this sense, the participation of a $T_2(\pi,\pi^*)$ state,[27] at the origin of the very fast ISC process (10^{11} s^{-1}) in benzophenone-like molecules (explaining the apparent violation of El-Sayed rules[14]), is therefore strongly expected also in the case of heterocyclic ketones. After formation of the $T_1(n,\pi^*)$ triplet state, the intramolecular[1,5] H sigmatropic shift proceeds very rapidly. Indeed, all values obtained from the Table 2 ($k_1 > 10^9$ s^{-1}) are higher than the 5×10^8 s^{-1} value for MBP[7]. This fast H atom transfer, which is sensitive to structural effects (QC18a vs QC18b as already discussed), points to an ideal conformation for γ-hydrogen abstraction and may reveal quantum tunneling[28] as is accepted for totally constrained photoenolizable molecules.[29] The most important reaction pathway for $T_1(n,\pi^*)$ is thus the production of the 1,4-biradical triplet photoenol species, ^{3}BR-E, and one would expect a two-step process: The sigmatropic shift forms a first biradical species (see the dashed line state in Figure 11) that evolves through bond rotation to allow the formation of an intramolecular hydrogen bonding with the adjacent carbonyl (suggested by solvent effects). However, the monoexponential kinetic appearance of ^{3}BR-E may indicate that H atom transfer is the limiting kinetic step while the bond rotation proceeds, therefore without encountering any significant potential barrier. The ^{3}BR-E is the precursor of CF in the case of QC1 and QC18a while for QC18b a back process to the

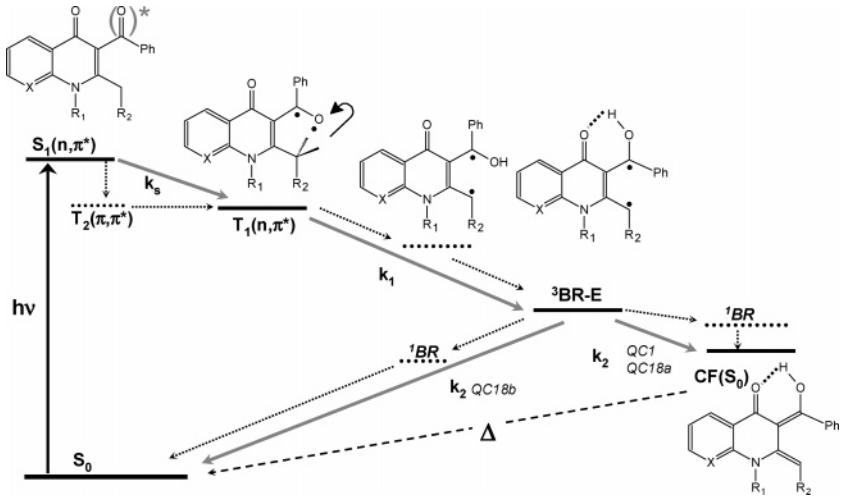

Figure 11. Overall reaction schemes describing the photoenolization process. Dashed line states and dashed line transitions (represented by arrows) are assumed to be involved in the reaction scheme but are not detected experimentally in this study.

CHART 2

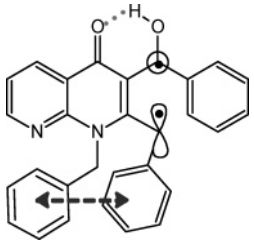

ground state of starting material (disproportionation process) is observed. It is well-known that the decay mechanism of a triplet biradical consists on the irreversible interconversion to a singlet biradicals (^{1}BR, on the Figure 11) that then yields products in a very fast process.[30] In our cases and for both deactivation channels (i.e., CF production or disproportionation), the experimental monoexponential decay of ^{3}BR-E of the three studied molecules (Table 3) is in conformity with the negligible lifetime (<1 ns[27,30]) of such singlet biradicals. However, a fundamental question still remains: Why is QC18b not photochromic even though ^{3}BR-E is clearly detected? Obviously, the comparison of QC18a and QC18b 1,4-biradicals is appropriate because the decisive role of the phenyl substituent in position 4 is clearly revealed. However, a simple substituent effect cannot be invoked to explain the different behavior of these two molecules if one reminds the example of *o*-methyl[7] and *o*-benzylbenzophenone[6] that give rise to 1,4-biradical upon photoexcitation as the precursor of the ground state photoenol. Alternatively, we think that additional conformational effects may play a decisive role in the fact that CF species is produced in QC18a but not in QC18b. Indeed, it is surprising that in spite of the presence of the supplementary stabilizing phenyl group (stabilization due to conjugation effect[31]), the lifetime of QC18a biradical is clearly shortened as compared to that of QC18b (Table 3). By analogy with previous results on simple photoenolizable valerophenone,[32] the steric interaction between the QC18a N-benzyl group and the other contiguous benzyl group may favor a molecular conformation allowing an ideal orientation of the atomic orbital at positions 1 and 4 maximizing the ISC process toward the CF species. In conformity with the classical picture of ISC process, such an ideal conformation corresponds to a perpendicular orientation of atomic p orbitals[31] as illustrated in Chart 2. The lack of photochromism of QC18b is a challenging question; therefore, theoretical calculations[9,27] would be very helpful to definitively address an answer.

Once it is produced, the CF species possesses a long lifetime due to intramolecular hydrogen bond stabilization and displays slow thermal back reactions in the dark.

Structural Factors Influencing the Photochromism. Finally, it is interesting to compare qualitatively the photochromic performances of QC1 and QC18a. According to the reaction scheme in Figure 11, the quantum yield for production of the colored form ϕ(CF) is proportional to $k_s \times k_1 \times k_2$. From the values located in Tables 2 and 3 for the different lifetimes, one estimates a ratio of 15:1 for the photochromic quantum yield in favor of QC18a. This drastic effect may be due to different (complementary) effects. First, the k_1 value for γ-hydrogen transfer is lower in QC1 as compared to that in QC18a. This difference suggests that (i) the biradical species is produced less efficiently in QC1 and (ii) structural effects should also play a non-negligible role in the rate of hydrogen transfer. In this sense, both steric (N−Me vs N−CH_2Ph) and electronic (quinolin-4-one vs naphthyridin-4-one) effects can be expected. Next, as proposed above, phenyl−phenyl interactions are absent (see Chart 2) for the biradical of QC1, which may explain its lower ISC rate (i.e., $k_2 \approx 1/\tau_2$) as compared with the more favorable value for QC18a. From the above example, it is clear that a better understanding of the photochemical step related to the photochromic yield can lead to intelligent optimization of photochromic performance. We conclude that QC18a is a better photochromic compound as compared to QC1.

Conclusions

Within the framework of a photochromism study, three photoenolizable heterocyclic ketones with the unique possibility of stabilizing the ground state photoenol by intramolecular hydrogen bond have been studied. For both the nonphotochromic QC18b molecule and the two photochromic QC18a and QC1 compounds, a clear picture of the full photochemical mechanism through the detection of all transient species has been established and summarized in Figure 11. Strong similarities between heterocyclic and simple photoenolizable ketones are found within the number, the nature of the transient species, and the processes involved. After photoexcitation, the first excited state $S_1(n,\pi^*)$ relaxes through an ISC process to the first excited triplet state $T_1(n,\pi^*)$ in which a [1,5]H sigmatropic shift takes place. This gives rise to 1,4-biradical species, identified also as a triplet photoenol species ^{3}BR-E. Either the CF species (for QC18a and QC1) or the ground state starting molecule (for

QC18b) is then produced. For both CF and ^{3}BR-E species, unexpected solvent effects are explained in terms of competition between intermolecular (solvent) and intramolecular (endo carbonyl group) hydrogen bonding. Because ^{3}BR-E is detected for all three compounds, it appears that the reactivity of this species controls the photochromism. Furthermore, it has been found that structural effects influence the γ-hydrogen abstraction as well as the biradical decay by ISC. With the idea of better controlling such effects to optimize the photochromic yield, the synthesis and investigation of new compounds are in course in our laboratories.

Acknowledgment. We are grateful to P. O'Keeffe for help with the revision of the English version. We thank the Groupement de Recherche GDR 2466 from CNRS and the Centre d'études et de Recherches Lasers et Applications (CERLA) for their help in the development of this work. CERLA is supported by the Ministère chargé de la Recherche, Région Nord/Pas de Calais, and the Fonds Européen de Développement Economique des Régions.

References and Notes

(1) Huffman, K. R.; Loy, M.; Ullman, E. F. *J. Am. Chem. Soc.* **1965**, *87*, 5417.

(2) Henderson, W. A., Jr.; Ullman, E. F. *J. Am. Chem. Soc.* **1965**, *87*, 5424.

(3) Yang, N. C.; Rivas, C. J. *J. Am. Chem. Soc.* **1961**, *83*, 2213.

(4) Sammes, P. G. *Tetrahedron* **1976**, *32*, 405.

(5) (a) Scaiano, J. C. *Acc. Chem. Res.* **1982**, *15*, 252. (b) Johnston, L. J.; Scaiano, J. C. *Chem. Rev.* **1989**, *89*, 521.

(6) (a) Netto-Ferreira, J. C.; Wintgens, V.; Scaiano, J. C. *Can. J. Chem.* **1994**, *72*, 1565. (b) Ohzeki, T.; Ohgusa, H.; Isaka, H.; Suzuki, S.; Takahashi, H. *Chem. Phys. Lett.* **1988**, *149*, 379.

(7) Nakayama, T.; Torii, Y.; Nagahara, T.; Hamanoue, K. *J. Photochem. Photobiol. A* **1998**, *119*, 1.

(8) Wagner, P. J.; Kelso, P. A.; Zepp, R. G. *J. Am. Chem. Soc.* **1972**, *94*, 7480.

(9) Wagner, P. J.; Sobczak, M.; Park, B. S. *J. Am. Chem. Soc.* **1998**, *120*, 2488.

(10) (a) Mal, P.; Lourderaj, U.; Venugopalan, P.; Moorthy, J. N.; Sathyamurthy, N. *J. Org. Chem.* **2003**, *68*, 3446. (b) Koner, A. L.; Singhal, N.; Nau, W. M.; Moorthy, J. N. *J. Org. Chem.* **2005**, *70*, 7439.

(11) Bouas-Laurent, H.; Dürr, H. *Photochromism*; Elsevier Science B. V.: Amsterdam, The Netherlands, 2003.

(12) (a) Valès, M. Ph.D. thesis, Université de Luminy, Marseille, 2001. (b) Valès, M.; Lokshin, V.; Pepe, G.; Guglielmetti, R.; Samat, A. *Tetrahedron* **2002**, *58*, 8543.

(13) Lokshin, V.; Valès, M.; Samat, A.; Pèpe, G.; Metelista, A.; Khodorkovsky, V. *Chem. Commun.* **2003**, 2080.

(14) Turro, N. J. *Modern Molecular Photochemistry*; The Benjamin/Cummings Publishing Co.: 1978.

(15) Redmond, R. W.; Scaiano, J. C. *J. Phys. Chem.* **1989**, *93*, 5347.

(16) Note that the reduction of the initial intensity in both the 640 and the 490 nm kinetics as the quencher concentration is raised, satisfactorily reproduced by the fits in Figure 8, is not due to a lowering of the initial T_B concentration but results from an effect of the convolution of the constant apparatus response with the increasingly rapid exponential decay kinetics of T_B (as the timescale of these kinetics are similar to the apparatus response time, its short-time region appears truncated).

(17) (a) Das, P. K.; Encinas, M. V.; Small, R. D., Jr.; Scaiano, J. C. *J. Am. Chem. Soc.* **1979**, *101*, 6965. (b) Baral-Tosh, S.; Chattopadhyay, S. K.; Das, P. K. *J. Phys. Chem.* **1984**, *88*, 1404.

(18) (a) Haag, R.; Wirz, J.; Wagner, P. J. *Helv. Chim. Acta* **1977**, *60*, 2595. (b) Lutz, H.; Bréhéret, E.; Lindqvist, L. *J. Chem. Soc. Faraday Trans. 1* **1973**, *69*, 2096.

(19) Kamlet, M. J.; Abboud, J. L.; Abraham, M. H.; Taft, R. W. *J. Org. Chem.* **1983**, *48*, 2877.

(20) Berthet, J.; Lokshin, V.; Valès, M.; Samat, A.; Vermeersch, G.; Delbaere, S. *Tetrahedron Lett.* **2005**, *46*, 6319.

(21) Delling, W. L. *J. Org. Chem.* **1966**, *31*, 1045.

(22) Scaiano, J. C. *J. Photochem.* **1973**, *2*, 81.

(23) If the triplet of the photoenol and the 1,4-biradical are one and the same species, the dominant character between radical-like or excited triplet state behavior (see ref 5) has to be determined although this information can only be precisely deduced from time-resolved ESR experiments. (a) Ikoma, T.; Akiyama, K.; Tero-Kubota, S.; Ikegami, Y. *J. Phys. Chem.* **1989**, *93*, 7087. (b) Akiyama, K.; Ikegami, Y.; Tero-Kubota, S. *J. Am. Chem. Soc*. **1987**, *109*, 2538.

(24) Quenching of type II biradical with β-carotene by triplet energy transfer is an example of excited state triplet behavior characterization. Kumar, C. V.; Chattopadhyay, S. K.; Das, P. K. *J. Am. Chem. Soc*. **1983**, *105*, 5143.

(25) De Feyter, S.; Diau, E. W.-G.; Zewail, A. H. *Angew. Chem. Int. Ed*. **2000**, *39*, 260.

(26) (a) Shah, B. K.; Rodgers, M. A. J.; Neckers, D. C. *J. Phys. Chem. A* **2004**, *108*, 6087. (b) McGarry, P. F.; Doubleday, C. E., Jr.; Wu, C.-H.; Staab, H. A.; Turro, N. J. *J. Photochem. Photobiol. A* **1994**, *77*, 109.

(27) The participation of the $T_2(\pi,\pi^*)$ state during Norrish type I and II reactions has been recently demonstrated by CASSCF calculation. He, H.-Y.; Fang, W.-H.; Philips, D. L. *J. Phys. Chem. A* **2004**, *108*, 5386.

(28) Wagner, P. J.; Giri, B. P.; Scaiano, J. C.; Ward, D. L.; Gabe, E.; Lee, F. E. *J. Am. Chem. Soc*. **1985**, *107*, 5490.

(29) (a) Sreedhara Rao, V.; Chandra, A. K. *Chem. Phys.* **1997**, *214*, 103. (b) Al-Soufi, W.; Eychmüller, A.; Grellmann, K. H. *J. Phys. Chem.* **1991**, *95*, 2022.

(30) Scaiano, J. C. *Tetrahedron* **1982**, *38*, 819.

(31) (a) Salem, L.; Rowland, C. *Angew. Chem., Int. Ed. Engl.* **1972**, *11*, 92. (b) Caldwell, R. A. *Pure Appl. Chem.* **1984**, *56*, 1167. The conjugation effect occurring during the biradical decay can be explained in the following terms: Increased delocalization should increase the average distance between the unpaired electrons of the biradical, thus lowering their spin-orbit coupling and consequently decreasing the yield of the ISC process responsible for the decay.

(32) Caldwell, R. A.; Majima, T.; Pac, C. *J. Am. Chem. Soc*. **1982**, *104*, 629.